



Stereolithographic hydrogel printing of 3D culture chips with biofunctionalized complex 3D perfusion networks

Zhang, Rujing; Larsen, Niels Bent

Published in:
Lab on a Chip

Link to article, DOI:
[10.1039/c7lc00926g](https://doi.org/10.1039/c7lc00926g)

Publication date:
2017

Document Version
Peer reviewed version

[Link back to DTU Orbit](#)

Citation (APA):
Zhang, R., & Larsen, N. B. (2017). Stereolithographic hydrogel printing of 3D culture chips with biofunctionalized complex 3D perfusion networks. *Lab on a Chip*, 17, 4273-4282. <https://doi.org/10.1039/c7lc00926g>

General rights

Copyright and moral rights for the publications made accessible in the public portal are retained by the authors and/or other copyright owners and it is a condition of accessing publications that users recognise and abide by the legal requirements associated with these rights.

- Users may download and print one copy of any publication from the public portal for the purpose of private study or research.
- You may not further distribute the material or use it for any profit-making activity or commercial gain
- You may freely distribute the URL identifying the publication in the public portal

If you believe that this document breaches copyright please contact us providing details, and we will remove access to the work immediately and investigate your claim.

Stereolithographic hydrogel printing of 3D culture chips with biofunctionalized complex 3D perfusion networks[†]

*Rujing Zhang, and Niels B. Larsen**

Department of Micro- and Nanotechnology, DTU Nanotech, Technical University of Denmark, 2800 Kgs. Lyngby, Denmark

E-mail: niels.b.larsen@nanotech.dtu.dk

Keywords: 3D printing, stereolithography, vascularization, hydrogels, tissue models

Abstract

Three-dimensional (3D) *in vitro* models capturing both the structural and dynamic complexity of the *in vivo* situation are in great demand as an alternative to animal models. Despite tremendous progress in engineering complex tissue/organ models in the past decade, approaches that support the required freedom in design, detail and chemistry for fabricating truly 3D constructs have remained limited. Here, we report a stereolithographic high-resolution 3D printing technique utilizing poly(ethylene glycol) diacrylate (PEGDA, MW 700) to manufacture diffusion-open and mechanically stable hydrogel constructs as self-contained chips, where confined culture volumes are traversed and surrounded by perfusable vascular-like networks. An optimized resin formulation enables printing of hydrogel chips holding perfusable microchannels with a cross-section as small as $100\ \mu\text{m} \times 100\ \mu\text{m}$, and the printed microchannels can be steadily perfused for at least one week. In addition, the

[†] Electronic supplementary information (ESI) available.

integration of multiple independently perfusable and structurally stable channel systems further allows for easy combination of different bulk material volumes at exact relative spatial positions. We demonstrate this structural and material flexibility by embedding a highly compliant cell-laden gelatin hydrogel within the confines of a 3D printed resilient PEGDA hydrogel chip of intermediate compliance. Overall, our proposed strategy represents an automated, cost-effective and high resolution technique to manufacture complex 3D constructs containing microfluidic perfusion networks for advanced *in vitro* models.

Introduction

In vitro models that recapitulate the complexity of *in vivo* tissues and organs have gained ever increasing attention for their use in a variety of biomedical applications such as drug development and toxicology, which can potentially replace expensive, time-consuming and controversial animal tests.^{1,2} As a result, the emerging field of “organs-on-chips” that integrate microfluidics with cell cultures have been continuously developed and shown to mimic important aspects of the biochemically dynamic characteristics *in vivo*.³⁻¹⁴ However, microfluidic systems are mostly engineered by soft lithography in polydimethylsiloxane (PDMS), which is labor intensive and usually can only produce microfluidic networks restricted to planar architectures that are inadequate to capture the intricacy of *in vivo* vascular networks.^{15,16} Additionally, PDMS permits significant diffusion of compounds in the vapor phase but not in the liquid phase.¹⁷ Consequently, cells are cultured in a volume where they are either directly exposed to fluid flow supplying oxygen and nutrients or shielded from direct convective flow by integrating extra structural elements such as micropillar arrays or porous membranes.^{12,18,19} Although direct exposure to shear

stress is desired for certain types of cells such as endothelial cells, most *in vivo* tissues are perfused through an independent pervasive vascular network. PDMS has also been reported to deplete the transported media of low polarity compounds by absorption, which can be troublesome for many applications.¹⁷ Therefore, new materials and methods for incorporating perfusable micro-channel networks of freely definable dense topology in diffusion-open and structurally stable materials are crucial for the development of advanced 3D *in vitro* models.

Recently, 3D printing or additive manufacturing has emerged as a promising and versatile tool to create true 3D constructs.²⁰ Extrusion-based printing, currently the most widely used technique in the field, has been utilized in combination with sacrificial molding to create vascularized tissue constructs by extrusion printing sacrificial filaments, such as carbohydrate glass,²¹ agarose²² and fugitive inks of Pluronic,^{23–25} that are later cast into cell-laden matrices. Direct extrusion printing of overhanging structures is challenging as extruded materials tend to fold or collapse under their own weight.²⁶ Hence, most vascular networks demonstrated in extrusion printing so far have been rectilinear lattice architectures with limited topological complexity.^{23,27–30} Furthermore, after the removal of sacrificial templates the formed channel networks are defined only by the matrices used for cell encapsulation, which are usually highly compliant hydrogels based on natural polymers such as collagen and gelatin.^{22–25} The latter materials are very well suited for 3D cell culture with *in vivo*-like mechanical properties and the possibility for cell-induced matrix remodeling, but the resulting constructs' high compliance and limited long-term structural fidelity and stability challenge their use as self-contained perfusable chip systems.

Our focus is to meet the challenge in establishing such mechanically stable, self-contained, densely 3D perfusable chip systems capable of supplying oxygen and

nutrients to an integrated 3D culture volume in a reproducible format and manufactured by a reproducible process. Direct high-resolution hydrogel printing of the perfusion channel walls instead of hydrogel casting of the walls onto printed sacrificial channel templates, as discussed above, will simplify the overall process with the caveat of fewer available wall materials. Stereolithography (SLA) has gained much interest due to its potential for 3D free-form printing at high spatial resolution in a parallel process to sustain useful volumetric print speeds.³¹⁻³³ SLA creates 3D constructs by light-induced solidification of a liquid resin layer-by-layer, most commonly by radical photopolymerization. So far, SLA based techniques have mostly been used for cell scaffolds with repetitive internal pore architectures such as woodpile, hexagonal or gyroid geometries, where transport of oxygen and nutrient is only mediated by passive diffusion instead of perfusion by convective flow.³⁴⁻³⁹ The use of SLA for *in vitro* models is still in its infancy, partly due to a shortage of demonstrated suitable cost-effective resins that can generate cell compatible, diffusion-open, and mechanically stable culture units.

We report the fabrication of SLA printed perfusion chip units where a confined cell culture volume is traversed and surrounded by perfusable vascular-like networks, as exemplified in Fig. 1a. By adopting medium molecular weight (MW) poly(ethylene glycol) diacrylate (PEGDA) for stereolithography, diffusion-open and mechanically stable self-contained perfusion chips are successfully manufactured. The resulting chips can subsequently easily be connected to an external pumping system through standard syringe needles and perfusion tubing. Steady perfusion of vascular-like channel networks and culture chambers through their respective sets of inlet and outlet, illustrated in green for the culture chamber and in red for the perfusion network in Fig. 1a, further allows the introduction of cell-laden matrices into geometrically

defined volumes of the culture chip with independently defined vascular microchannel networks.

Results and discussion

Choice of resin components

An aqueous pre-polymer solution composed of monomer (PEGDA, M_n 700 g mol⁻¹), photoinitiator (lithium phenyl-2,4,6-trimethylbenzoylphosphinate, LAP) and photoabsorber (quinoline yellow, QY) was employed for stereolithography. PEGDA, a synthetic polymer, has commonly been used for cell encapsulation in biomedical studies due to its cell compatibility and non-fouling property. Cell encapsulation typically uses higher MW PEGDA ($M_n > 2000$ g mol⁻¹) since the resulting more compliant hydrogels of lower cross-linking density permit cells to proliferate and migrate.³⁹⁻⁴¹ Other researchers have used undiluted highly crosslinked low MW PEGDA (M_n 250 g mol⁻¹) to manufacture microfluidic devices that resist swelling and are impermeable to water, and consequently impermeable to water-soluble nutrients.⁴²⁻⁴⁴ Our aim is to manufacture the perfusion chip unit surrounding the encapsulated cells, and we consequently selected a medium MW PEGDA to produce mechanically stable, yet diffusion-open, compliant hydrogel constructs.⁴⁵ LAP and QY were selected because of their excellent water solubility and low cytotoxicity.^{45,46} The photoabsorber was used to limit the light penetration into the pre-polymer solution and thereby to achieve an optical Z resolution of the printer by matching its concentration to the printing process, as discussed in detail below. Importantly, printing in aqueous solution minimizes dimensional changes caused by post-printing swelling. The printed hydrogels reach their equilibrium slightly swollen state within 4 h after being transferred to a water bath (Fig. S1 in the ESI).

Perfusion of printed PEGDA microchannels with full 3D design freedom

First, we verified that printed fluidic networks can easily and stably be perfused. Blunt needles, mounted to flexible micro-tubing connected to an external peristaltic pump, are inserted into printed channel connectors (Fig. 1b,c). The connector inner diameter (0.7 mm) is designed to be slightly smaller than the needle outer diameter (0.8 mm) to enable a tight seal to the needle. The printed PEGDA hydrogels of shear modulus ~ 0.4 MPa (Fig. S2) withstand the needle insertion and form tight seals.^{22,43} Simultaneous independent perfusion of the separate channels of a dual channel scaffold is thus achieved (Fig. 1d, Movie S1). Stable leak-free perfusion for at least one week is routinely observed, documented by time-lapse video of steady-state diffusion concentration gradients of a perfused dye solution across the channel walls (Movie S2). Second, we printed a series of channel systems with increasing 3D complexity, which were afterwards successfully perfused (Fig. 1e-g, Movie S3-5). These results show that perfusable channels with full 3D design freedom are easily accessible by our approach, while being a significant challenge using current PDMS-based microfluidic manufacturing processes.

Optimization of the spatial printing resolution for microchannels

Next, we explored the spatial resolution of the printer setup to address the difficulty in fabricating small diameter channels that are physiologically relevant ($\varnothing < 500 \mu\text{m}$).²⁶ The concept of stereolithographic printing resolution is not consistently considered in the literature where the reported achievable spatial resolution often refers to the level of detail of open-surface features instead of closed channel structures.⁴⁷ A more relevant resolution assessment of channel structures is the deviation of the printed

dimensions of a sealed perfusable channel from the design dimensions.^{42,47} The distinction between open and closed channels using stereolithography is important, since the structural fidelity of a closed rectangular channel largely depends on the light penetration depth into the pre-polymer solution (*Z* resolution), while that of an open channel mainly depends on *XY* resolution pre-determined by the light exposure units of the printer. Deep light penetration leads to mechanically stable structures by ensuring strong bonding between neighboring layers (penetration into the previously formed layers), but also causes over-curing of the channel ceiling into the channel volume (penetration into the pre-polymer/uncured solution). Over-curing results in reduced vertical dimensions and sometimes even occlusion of the channel. By proper selection of the photoabsorber and its concentration, light penetration can be controlled to well match the layer thickness used for printing so that strong bonding between neighboring layers can be achieved with minimized over-curing. We investigated this combined effect of absorber concentration and layer thickness on the spatial resolution of the printed object by first printing sealed channels of square cross-sections at different absorber concentrations and subsequently characterizing both their horizontal and vertical dimensions. Optical microscopy of cross-sectioned printed channels show that channels as small as $100\ \mu\text{m} \times 100\ \mu\text{m}$ can be printed using a layer thickness of $25\ \mu\text{m}$ and medium absorber concentration ($9\ \text{mg/mL}$). Use of a lower absorber concentration ($6\ \text{mg/mL}$) leads to complete occlusion of $100\ \mu\text{m} \times 100\ \mu\text{m}$ channels as well as substantial reduction in vertical dimensions of larger channels (Fig. 2a,b; darker areas as explained in the Materials and methods section). Despite well-defined features of the printed $100\ \mu\text{m} \times 100\ \mu\text{m}$ channels using $9\ \text{mg/mL}$ absorber, as observed by optical microscopy, the resulting channels could not be perfused. A higher absorber concentration ($12\ \text{mg/mL}$) was employed to minimize

the risk of random channel occlusion but this resulted in mechanically unstable structures (data not shown). The layer thickness was then decreased from 25 μm to 20 μm to enhance the bonding between neighboring layers and consequently robust structures were successfully printed using 12 mg/mL absorber. With the optimized resin and printing procedure, microfluidic channels with cross-sections of 100 μm \times 100 μm can be faithfully printed (Fig. 2a,c) and are fully functional, as demonstrated by successful perfusion of a single channel stepwise narrowing from a cross-section of 400 μm \times 400 μm to 100 μm \times 100 μm after printing (Fig. 2d). Native vascular networks use circular channel geometries that lead to homogenous wall shear stress, in contrast to the variable wall shear stress in rectangular channels.⁴⁸ Therefore, we also evaluated printing of circular geometries of decreasing diameters using optimized resin formulation. The resulting channel cross-sections are well defined, although the intrinsic grid geometry of the light exposure unit (a Digital Mirror Device) causes jagged perimeters of the smallest diameter designs (Fig. S3). To our best knowledge, few reports have shown the printing of perfusable freely designable micro-channels approaching the dimensions of larger arterioles and venules⁴⁹ in hydrogel materials.

Cell compatibility of the printed micro-perfusable chip constructs

We first investigated the cell compatibility of SLA printed bowl-shaped constructs (Fig. 3a). Bowl structures were used since their overall planar bottom surface, without or with printed open channel structures, greatly facilitated visualization by microscopy of the cell number and distribution compared to closed microchannels. Endothelial cells were used because ideally they should line the synthetic vascular-like channel wall to regulate solute transport and facilitate homeostasis as in the *in vivo* situation.⁵⁰ Prior to seeding, the surfaces of printed constructs were

functionalized with cell adhesive gelatin-based ligands since pristine PEGDA hydrogel surfaces do not support cell attachment (Fig. S4). Gelatin methacrylate (GelMA) is widely used as a photocrosslinkable hydrogel matrix for accommodating live cells.⁵¹ PEGDA structures with pendant unreacted acrylate groups were exposed to LAP-containing GelMA solution and subsequently to UV-A illumination. Seeded Human umbilical vein endothelial cells (HUVEC) adhered and assembled into a nearly confluent layer with negligible observable cell death after culture for 24 h (Fig. 3b; Fig. S5), in support of the cell compatibility of the printed and modified constructs. Next, we printed and exposed a circular channel ($\text{\O} 300 \mu\text{m}$) with its inner wall functionalized with GelMA to a HUVEC cell suspension by perfusion. The use of a low GelMA concentration (10 mg mL^{-1}) resulted in specific channel wall functionalization without unwanted bulk GelMA hydrogel formation in the fluidic channels.⁵² After incubation for 24 h HUVEC cells lined the vessel-like wall (Fig. 3c,d). This demonstrates the applicability of our light-based synthetic hydrogel printing and biofunctionalization approach to produce *in vitro* endothelialized fluidic channel systems with physiological complexity. It should be noted that the printed PEGDA walls will allow for diffusive paracrine signaling but not for direct cell-cell contact between the endothelial cells in the channel systems and the cells cultured in a separate printed compartment. This is current limitation of the system, which may be circumvented in future designs by including micro-fenestrations in the printed channel designs, as demonstrated previously in 2D microfluidic vessel models.⁵³

Embedding of cell-laden matrices with separate vascular-like microfluidic networks

We finally fabricated a true 3D chip unit with separate cell culture chamber and vascular-like fluidic networks, as illustrated in Fig. 1a, to address the current fabrication limitations for creating advanced *in vitro* models. The central culture chamber is surrounded by a multi-furcated perfusion network composed of 8 circular channels ($\sim \text{Ø } 200 \text{ }\mu\text{m}$) and traversed by a center channel ($\text{Ø } 180 \text{ }\mu\text{m}$, Fig. 4a,b) only supported by a narrow bridge with diamond shaped fenestrations (Fig. 4a insert). This design enables tissue cells to reside on all sides of the center channel. First, the independent perfusion of the channel network and the culture chamber using aqueous dye solutions demonstrates the ability to introduce different materials into distinct chip construct volumes (Fig. 4c). The observed slight blur along the chamber and channel perimeters is caused by fast diffusion of the small dye molecules into the surrounding diffusion-open PEGDA hydrogel in the time between loading the channels and recording the micrograph. Next, we separately perfused the channel network with LAP-containing acrylated rhodamine solution and the chamber with GelMA solution containing LAP and live-stained 3T3 fibroblasts. Subsequent UV-A illumination of the printed device shortly after perfusion induced immobilization of the rhodamine molecules diffused into the walls of the channel network through covalent binding as well as cross-linking of the cell-laden GelMA hydrogel in the culture chamber. Confocal imaging confirmed the coexistence of perfused fluidic channels and encapsulated live cells (Fig. 4d,f). All channels of the vessel network were perfused, as evidenced by the cross-sectional view of the red fluorescence from bound rhodamine displayed in Fig. 4e. After the demonstration of chamber loading and channel network perfusion, long-term perfusion cultures were performed using such 3D culture chips. A higher fraction of live cells were observed after a week-long culture in the chips that were continuously perfused compared to the ones cultured in

a static condition (Fig. S6), indicating soluble factors such as oxygen and nutrients can continuously diffuse into the culture chamber mediated by perfusion and consequently maintain a healthier cell culture in the long term. Our approach can easily be scaled up and potentially be used to culture multiple cell types by printing different culture volumes that are supplied and fluidically connected by the embedded vascular-like networks at exact relative spatial positions within a single chip device, which could serve as advanced *in vitro* models where the systemic effect of a drug can be studied. Furthermore, based on long-term steady perfusion as well as predictable diffusion kinetics, compound diffusion through channel network to culture volume and subsequently within cellular matrices can be well modeled and manipulated using our printed hydrogel chip systems. Such control over various physiochemical conditions such as oxygen tension and chemical gradients in cellular microenvironment can potentially enable studies on the effect of specific environmental cues on cellular behaviors.

Conclusions

In summary, we have developed a new approach based on high-resolution stereolithography employing easily synthesized and commercially available starting compounds to produce *in vitro* vascular network-like hydrogel constructs with high 3D complexity, facile perfusion setup, and the possibility to culture cells in both the vascular networks and the defined interstitial volumes. In addition, this technique is suitable for production up-scaling without compromising spatial resolution and fabrication speed with the continuous advances in optical components developed for SLA. Further work should be performed to validate the proposed approach with respect to its use as fully functional *in vitro* models. Future studies will focus on

detailed investigation of long-term cell culture behavior in 3D when the chemical microenvironment is modulated by compound perfusion through the vascular network-like constructs. This versatile platform opens new avenues for a number of biomedical applications, such as chemotaxis studies, drug development and *in vitro* disease modeling.

Materials and methods

Materials

Poly(ethylene glycol) diacrylate (M_n 700 g mol⁻¹, PEGDA) and Quinoline Yellow (QY) were acquired from Sigma-Aldrich and used as purchased.

LAP Synthesis

LAP was synthesized based on a previously reported procedure.⁴⁶ Briefly, at room temperature and in a nitrogen atmosphere, 3.2 g of 2,4,6-trimethylbenzoyl chloride (TCI America) was added dropwise to an equimolar amount of continuously stirred dimethyl phenylphosphonite (3.0 g, Sigma-Aldrich). The reaction mixture was stirred overnight, followed by the addition of a four-fold excess of lithium bromide (6.1 g, Sigma-Aldrich) dissolved in 100 mL acetone. The reaction mixture was then heated to 50 °C. After about 10 min, a white solid precipitate formed. The mixture was cooled to room temperature and then filtered under vacuum. The filtrate was washed 3 times with acetone to remove unreacted lithium bromide, and the remaining solvent was removed by vacuum.

GelMA Synthesis

GelMA was synthesized based on a previously reported procedure.²³ Briefly, a 100 mg mL⁻¹ gelatin solution was first prepared by dissolving gelatin powder (Type A, 300 g bloom from porcine skin, Sigma-Aldrich) in Dulbecco's phosphate-buffered saline (DPBS) at 60 °C for 2 h with vigorous stirring. Then the solution temperature was lowered to 50 °C and 0.14 mL of methacrylic anhydride was added dropwise to the gelatin solution for each gram of gelatin in the solution (about 50% degree of methacrylation). The mixture was allowed to react for 4 h at 50 °C with vigorous stirring. The methacrylation reaction was then quenched by diluting the mixture with DPBS pre-warmed to 40 °C to a GelMA concentration of 45 mg mL⁻¹. GelMA was precipitated overnight by the addition of 100 mL ice-cold acetone to the diluted mixture. Acetone was then decanted from the precipitated GelMA, which was then dissolved in DPBS at 100 mg mL⁻¹ at 40 °C. The warm GelMA solution was filtered under vacuum through a 0.2 µm filter (PES membrane, VWR vacuum filtration), transferred to a 12-14 kDa molecular weight cutoff (MWCO) dialysis tubing (Spectra/Por 4), and dialyzed against deionized (DI) water at 40 °C for 3 days with frequent change of the dialysis media (twice a day) to remove remaining methacrylic acid. Finally, the GelMA was lyophilized for 2 days and subsequently stored at -20 °C prior to further use.

Activation of Cover Glass Surfaces

The PEGDA hydrogels were printed onto pre-treated cover glasses for the purpose of easy handling, calling for prior chemical activation of the glass surface to secure the printed PEGDA to the glass support. The treatment was based on a previously reported procedure.⁵⁴ The circular cover glasses (Ø 20 mm, VWR) were first cleaned via plasma treatment to remove organic contaminants. The cleaned glasses were then

soaked in a 2% v/v 3-(trimethoxysilyl)propyl methacrylate (Sigma-Aldrich) solution in 95% v/v ethanol/water (pH adjusted to 5 by acetic acid) for 10 min, washed with pure ethanol for 3 times, and eventually baked at 105 °C for another 10 min.

Projection Stereolithography of PEGDA Hydrogels

Stereolithographic printing used a home-built high resolution printer based on 1-to-1 projection of light reflected off a Digital Mirror Device (13.68 μm pixel pitch, DLP7000 UV, Texas Instruments, DMD) coupled to a V-7000 Hi-Speed controller (Vialux). The printing process proceeded using custom written MATLAB (MathWorks) code that synchronizes digital mask exposure on the DMD, light exposure using a 365-nm high power LED (LZ1-00UV00, Ledengin), and fabrication stage movement via a linear stage (LNR50S, Thor Labs). The power density at the vat bottom was 10.9 mW cm^{-2} as measured using a UV power meter (OAI 306, Optical Associates). Pre-treated cover glasses were mounted to the fabrication stage. Non-adhesive fluorinated ethylene propylene (FEP) foil was applied to the vat bottom to facilitate smooth release of each printed layer from the vat. 3D models were designed using Autodesk Inventor 2016 (Autodesk). The resulting design was sliced into a series of digital masks with a slicing thickness of 20 μm using the open-source slicer software Slic3r. The aqueous resin consisted of 200 mg mL^{-1} PEGDA, 5 mg mL^{-1} LAP and 12 mg mL^{-1} QY. After adding resin to the vat, the fabrication stage was moved close to the vat bottom. The first digital mask was projected for an extended time of 15 s to ensure proper attachment of the polymer to the cover glass. After the formation of the first layer, the stage was raised by 20 μm for each additional digital mask exposure. The first 10 layers (corresponding to ~ 200 μm thickness) were each exposed for 15 s followed by a gradual reduction of the exposure time to 3 s over the

next 10 layers to minimize mechanical strain. All layers in the remaining part of the printed object, including all parts defining channel and chamber structures, were exposed for 3 s each. After printing, the object was immediately immersed in DI water for at least overnight to leach out remaining reagents and allowing it to reach its equilibrium swollen state prior to further use.

Cross-sectional Analysis of Printed Channels

Printed PEGDA hydrogel with square channels of varying dimensions were mechanically cut by a razor blade to allow for optical inspection of the channel shapes, as reported in Fig. 2. Light will only be transmitted through the open channels during optical analysis if the axial channel orientation is exactly parallel to the impinging light rays, leading to random variations between cut samples in the channels appearing brighter or darker than the surrounding printed PEGDA in the acquired optical micrographs, depending on two cut faces being exactly parallel and exactly perpendicular to the channel orientation. These variations are reflected in channels appearing darker in Fig. 2b and brighter in Fig. 2c. Optical analysis was in general found to be inadequate for reliable evaluation of the channel perfusability.

Perfusion of Printed PEGDA Microchannel Networks

Blunt stainless needles ($\text{\O} 0.8 \text{ mm} \times 22 \text{ mm}$, Sterican) were mounted to polytetrafluoroethylene (PTFE) tubing ($\text{\O}_{\text{inner}} 0.30 \text{ mm}$ and $\text{\O}_{\text{outer}} 0.50 \text{ mm}$, Adtech Polymer Engineering) that was connected to a peristaltic pump (MasterFlex) via Luer Lock connectors. Printed constructs were fixated onto the bottom of a polystyrene petri dish using double sided adhesive tapes, and the petri dish filled with DI water. Aqueous solutions of either red or blue food dye (Dr. Oetker) were used as perfusion

fluids. The tubing was pre-perfused with fluid, and the needles were inserted into the 3D printed inlet and outlet ($\text{\O} 0.7 \text{ mm}$). Pumping proceeded at a flow rate of $100 \mu\text{L min}^{-1}$ and the channel perfusion was recorded by a phone camera. The recorded videos were stabilized using the plugin TurboReg in the Fiji software package.^{55,56}

Cell Culture

Primary human umbilical vein endothelial cells (HUVECs) (Gibco) were cultured in Medium 200 (Gibco) supplemented with 2% v/v Large Vessel Endothelial Supplement (Gibco). 3T3 Swiss Albino cells (ECACC 85022108) were cultured in Dulbecco's modified Eagle's medium with high glucose (DMEM, Biowest) supplemented with 10% v/v fetal bovine serum (FBS, Sigma-Aldrich) and 1% v/v penicillin-streptomycin (P/S, Sigma-Aldrich). All the cell cultures were passaged following the respective vendors' manuals. HUVECs were not used beyond passage 5.

Cytotoxicity Assay

Bowl structures ($\text{\O}_{\text{inner}} 8 \text{ mm}$, $\text{\O}_{\text{outer}} 10 \text{ mm}$, 0.4 mm thick bottom, 2.5 mm overall height) were printed and immersed in DI water for 24 h with two intermediate changes of water bath to allow the leaching of unreacted reagents. 100 μL aqueous solution of 10 mg mL^{-1} GelMA and 5 mg mL^{-1} LAP was added to each bowl, followed by 2 min of UV-A illumination (330-380 nm, peaking at 365 nm, 18 mW cm^{-2}).⁵⁷ The reaction mixture was removed and the structures were washed with DI water 3 times before being immobilized in a 6-well plate using double sided adhesive tape. HUVEC culture medium was added to the well plate to submerge each structure and the whole plate containing the structures was sterilized by 20 min exposure of UV-C irradiation (254 nm, UV sterilization cabinet, Cleaver Scientific) in a laminar

flow bench. The structures were immersed in HUVEC culture medium overnight to exchange the water in the hydrogel for culture medium. Before cell seeding, culture medium was partially removed so that each bowl structure was not submerged yet still moist. Then the culture medium inside each bowl was replaced with 100 μL HUVEC suspension. Cells were seeded at three densities, 7×10^4 cells cm^{-2} , 1.4×10^5 cells cm^{-2} , and 2.1×10^5 cells cm^{-2} , respectively, and cultured at 37 °C in 5% CO_2 for 24 h. Non-adherent cells were washed away using culture medium, and adhered cells were stained with calcein-AM (2 $\mu\text{g mL}^{-1}$, Invitrogen), propidium iodide (PI, 2 $\mu\text{g mL}^{-1}$, Sigma-Aldrich) and Hoechst 33342 (2 $\mu\text{g mL}^{-1}$, Sigma-Aldrich) for 1 h. Each sample was then characterized by fluorescence microscopy (AxioVert 100 M, Zeiss). Composite microscopy images were generated using Fiji by combining the three fluorescence channels.

Endothelialization of Perfusion Channels

The inner walls of printed vascular channels were functionalized by perfusing 0.5 mL aqueous solution of 10 mg mL^{-1} GelMA and 10 mg mL^{-1} LAP, followed by 2 min of UV-A illumination. Constructs were then immersed in HUVEC culture medium, sterilized by UV-C irradiation for 20 min in a laminar flow bench, and stored overnight. The functionalized channels were perfused with 0.5 mL HUVEC suspension (1×10^7 cells mL^{-1}). The petri dish containing the construct was then fully filled with culture medium, sealed using Parafilm, and fixated onto the bottom of an acrylic box. Fast cell sedimentation in the channel leading to inhomogeneous cell coverage was overcome by repeated rotation of the construct around the channel axis during the seeding process: The box was initially turned upside down and incubated for 15 min. The box was rotated 90° clockwise and again incubated for 15 min, and

then rotated 180° counter-clockwise before incubating for another 15 min. The same cycle was conducted again to ensure that all parts of the channel walls were fully exposed to the cells. After 24 h incubation at 37 °C and 5% CO₂, the channels seeded with HUVECs were perfused with 0.5 mL of culture medium containing 2 µg mL⁻¹ calcein-AM and further incubated for 1 h. The samples were then characterized by confocal laser scanning microscope (LSM 700, Zeiss) using excitation at 488 nm. The vertical axis of the acquired confocal z-stack micrographs was corrected for the refractive index of the culture medium using the microscope software package (Zeiss Zen 2012 Black edition).

Multi-furcated 3D perfusion culture constructs

Constructs with a separate culture chamber and channel networks were printed in PEGDA. The channels were first perfused with 1 mL of 20 µg mL⁻¹ acryloxyethyl thiocarbamoyl rhodamine B (Sigma-Aldrich) solution containing 10 mg mL⁻¹ LAP, followed by 2 min of UV-A illumination. The unreacted rhodamine molecules were flushed away using DI water. The constructs were then immersed in 3T3 fibroblast culture medium overnight to exchange the DI water for medium in the PEGDA hydrogel. Before harvesting cells, 3T3 fibroblasts were stained with calcein-AM (2 µg mL⁻¹) in a culture flask for 1 h. Cell-laden GelMA solution was prepared by mixing warm (37 °C) LAP-containing GelMA solution in DPBS with an equivalent volume of 3T3 fibroblast suspension to reach final concentrations of 100 mg mL⁻¹ GelMA, 5 mg mL⁻¹ LAP and 5 × 10⁶ cells mL⁻¹. The culture chamber was then perfused with 0.5 mL of cell-laden GelMA solution, followed by 90 s of UV-A illumination. Both the intact sample and cross-sectional slices generated by manual cutting were then

characterized by confocal laser scanning microscopy using excitation at 405, 488, and 555 nm.

Analysis of swelling properties

Solid PEGDA objects of size 10 mm × 10 mm × 3.5 mm were printed on a cover glass by stereolithography employing the same pre-polymer solution composition and printing conditions used for printing perfusion constructs. Immediately after printing, surplus water was removed by quickly touching the cuboid's surfaces with tissue, and its weight was determined. The sample was immediately reimmersed in DI water, and the procedure was repeated after 1, 2, 3, 4 h as well as after overnight immersion. The swollen cuboid was placed in an oven at 140 °C and the weight after overnight drying was used for calculating the volumetric swelling ratio (Fig. S1).

Analysis of mechanical properties

Solid PEGDA cylinders of Ø 6 mm and height 5 mm were printed on a cover glass by stereolithography employing the same pre-polymer solution composition and printing conditions used for printing perfusion constructs. The printed cylinders were released from the cover glass support by a scalpel and allowed to reach their equilibrium degree of swelling by immersion overnight in DI water. The mechanical properties of the still wet samples were analyzed on an Instron 5967 at a compression rate of 0.5 mm min⁻¹ to a final extension ratio λ of 0.7. The data was analyzed using neo-Hookean rubber elastic theory for highly swollen hydrogels that predicts a linear dependence of the stress on $\lambda-\lambda^{-2}$.⁵⁸ The results are displayed in Fig. S2, where a linear fit to the data in the $\lambda-\lambda^{-2}$ range from 0.2 to 0.8 yields a hydrogel shear modulus of 0.43 MPa.

Acknowledgements

The authors kindly acknowledge financial support from DTU Nanotech, Technical University of Denmark.

References

- 1 J. Jang, H.-G. Yi and D.-W. Cho, *ACS Biomater. Sci. Eng.*, 2016, **2**, 1722–1731.
- 2 R. Edmondson, J. J. Broglie, A. F. Adcock and L. Yang, *Assay Drug Dev. Technol.*, 2014, **12**, 207–218.
- 3 A. Hasan, A. Paul, A. Memic and A. Khademhosseini, *Biomed. Microdevices*, 2015, **17**, 1–13.
- 4 B. N. Johnson, K. Z. Lancaster, I. B. Hogue, F. Meng, Y. L. Kong, L. W. Enquist and M. C. McAlpine, *Lab Chip*, 2016, **16**, 1393–1400.
- 5 Y. Huang, J. C. Williams and S. M. Johnson, *Lab Chip*, 2012, **12**, 2103–2117.
- 6 H. J. Kim, D. Huh, G. Hamilton and D. E. Ingber, *Lab Chip*, 2012, **12**, 2165–2174.
- 7 A. Grosberg, P. W. Alford, M. L. McCain and K. K. Parker, *Lab Chip*, 2011, **11**, 4165–4173.
- 8 K. E. Sung, N. Yang, C. Pehlke, P. J. Keely, K. W. Eliceiri, A. Friedl and D. J. Beebe, *Integr Biol*, 2011, **3**, 439–450.
- 9 D. Huh, G. A. Hamilton and D. E. Ingber, *Trends Cell Biol.*, 2011, **21**, 745–754.
- 10 K. Domansky, W. Inman, J. Serdy, A. Dash, M. H. M. Lim and L. G. Griffith, *Lab Chip*, 2010, **10**, 51–58.
- 11 K.-J. Jang and K.-Y. Suh, *Lab Chip*, 2010, **10**, 36–42.
- 12 D. Huh, B. D. Matthews, A. Mammoto, M. Montoya-Zavala, H. Y. Hsin and D.

- E. Ingber, *Science*, 2010, **328**, 1662–1668.
- 13 V. van Duinen, S. J. Trietsch, J. Joore, P. Vulto and T. Hankemeier, *Curr. Opin. Biotechnol.*, 2015, **35**, 118–126.
- 14 E. K. Sackmann, A. L. Fulton and D. J. Beebe, *Nature*, 2014, **507**, 181–189.
- 15 N. Bhattacharjee, A. Urrios, S. Kang and A. Folch, *Lab Chip*, 2016, **16**, 1720–1742.
- 16 S. Halldorsson, E. Lucumi, R. Gómez-Sjöberg and R. M. T. Fleming, *Biosens. Bioelectron.*, 2015, **63**, 218–231.
- 17 N. Li, M. Schwartz and C. Ionescu-Zanetti, *J. Biomol. Screen.*, 2009, **14**, 194–202.
- 18 G. M. Walker, H. C. Zeringue and D. J. Beebe, *Lab Chip*, 2004, **4**, 91–97.
- 19 L. Kim, Y. Toh, J. Voldman and H. Yu, *Lab Chip*, 2007, **7**, 681–694.
- 20 S. Waheed, J. M. Cabot, N. P. Macdonald, T. Lewis, R. M. Guijt, B. Paull and M. C. Breadmore, *Lab Chip*, 2016, **16**, 1993–2013.
- 21 J. S. Miller, K. R. Stevens, M. T. Yang, B. M. Baker, D.-H. T. Nguyen, D. M. Cohen, E. Toro, A. A. Chen, P. A. Galie, X. Yu, R. Chaturvedi, S. N. Bhatia and C. S. Chen, *Nat. Mater.*, 2012, **11**, 768–774.
- 22 L. E. Bertassoni, M. Cecconi, V. Manoharan, M. Nikkhah, J. Hjortnaes, A. L. Cristino, G. Barabaschi, D. Demarchi, M. R. Dokmeci, Y. Yang and A. Khademhosseini, *Lab Chip*, 2014, **14**, 2202–2211.
- 23 D. B. Kolesky, R. L. Truby, A. S. Gladman, T. A. Busbee, K. A. Homan and J. A. Lewis, *Adv. Mater.*, 2014, **26**, 3124–3130.
- 24 D. B. Kolesky, K. A. Homan, M. A. Skylar-Scott and J. A. Lewis, *Proc. Natl. Acad. Sci. U. S. A.*, 2016, **113**, 3179–3184.
- 25 Y. S. Zhang, F. Davoudi, P. Walch, A. Manbachi, X. Luo, V. Dell’Erba, A. K.

- Miri, H. Albadawi, A. Arneri, X. Li, X. Wang, M. R. Dokmeci, A. Khademhosseini and R. Oklu, *Lab Chip*, 2016, **16**, 4097–4105.
- 26 I. S. Kinstlinger and J. Miller, *Lab Chip*, 2016, **16**, 2025–2043.
- 27 D. B. Kolesky, K. A. Homan, M. A. Skylar-Scott and J. A. Lewis, *Proc. Natl. Acad. Sci. U. S. A.*, 2016, **113**, 3179–84.
- 28 C. Colosi, S. R. Shin, V. Manoharan, S. Massa, M. Costantini, A. Barbetta, M. R. Dokmeci, M. Dentini and A. Khademhosseini, *Adv. Mater.*, 2016, **28**, 677–684.
- 29 J. W. Lee, Y.-J. Choi, W.-J. Yong, F. Pati, J.-H. Shim, K. S. Kang, I.-H. Kang, J. Park and D.-W. Cho, *Biofabrication*, 2016, **8**, 15007.
- 30 H.-W. Kang, S. J. Lee, I. K. Ko, C. Kengla, J. J. Yoo and A. Atala, *Nat. Biotechnol.*, 2016, **34**, 312–319.
- 31 F. P. W. Melchels, J. Feijen and D. W. Grijpma, *Biomaterials*, 2010, **31**, 6121–6130.
- 32 T. Billiet, M. Vandenhaute, J. Schelfhout, S. Van Vlierberghe and P. Dubruel, *Biomaterials*, 2012, **33**, 6020–6041.
- 33 J. R. Tumbleston, D. Shirvanyants, N. Ermoshkin, R. Januszewicz, A. R. Johnson, D. Kelly, K. Chen, R. Pinschmidt, J. P. Rolland, A. Ermoshkin, E. T. Samulski and J. M. DeSimone, *Science*, 2015, **347**, 1349–1352.
- 34 S. P. Grogan, P. H. Chung, P. Soman, P. Chen, M. K. Lotz, S. Chen and D. D. D’Lima, *Acta Biomater.*, 2013, **9**, 7218–7226.
- 35 L.-H. Han, S. Chen, G. Mapili and K. Roy, *J. Manuf. Sci. Eng.*, 2008, **130**, 21005.
- 36 S. J. Leigh, H. T. J. Gilbert, I. A. Barker, J. M. Becker, S. M. Richardson, J. A. Hoyland, J. A. Covington and A. P. Dove, *Biomacromolecules*, 2013, **14**, 186–

- 192.
- 37 H. Lin, D. Zhang, P. G. Alexander, G. Yang, J. Tan, A. W.-M. Cheng and R. S. Tuan, *Biomaterials*, 2013, **34**, 331–339.
- 38 L. Elomaa, S. Teixeira, R. Hakala, H. Korhonen, D. W. Grijpma and J. V. Seppälä, *Acta Biomater.*, 2011, **7**, 3850–3856.
- 39 J. P. Mazzoccoli, D. L. Feke, H. Baskaran and P. N. Pintauro, *J. Biomed. Mater. Res. - Part A*, 2010, **93**, 558–566.
- 40 L. M. Weber, C. G. Lopez and K. S. Anseth, *J. Biomed. Mater. Res. Part A*, 2009, **90A**, 720–729.
- 41 I. Mironi-Harpaz, D. Y. Wang, S. Venkatraman and D. Seliktar, *Acta Biomater.*, 2012, **8**, 1838–1848.
- 42 H. Gong, M. Beauchamp, S. Perry, A. T. Woolley and G. P. Nordin, *RSC Adv.*, 2015, **5**, 3627–3637.
- 43 A. Urrios, C. Parra-Cabrera, N. Bhattacharjee, A. M. Gonzalez-Suarez, L. G. Rigat-Brugarolas, U. Nallapatti, J. Samitier, C. A. DeForest, F. Posas, J. L. Garcia-Cordero and A. Folch, *Lab Chip*, 2016, **16**, 2287–2294.
- 44 H. Gong, B. P. Bickham, A. T. Woolley and G. P. Nordin, *Lab Chip*, 2017, **17**, 2899–2909.
- 45 A. Faralli, F. Melander, E. K. U. Larsen, S. Chernyy, T. L. Andresen and N. B. Larsen, *Adv. Healthcare Mater.*, 2016, **5**, 244–254.
- 46 B. D. Fairbanks, M. P. Schwartz, C. N. Bowman and K. S. Anseth, *Biomaterials*, 2009, **30**, 6702–6707.
- 47 A. Urrios, C. Parra-Cabrera, N. Bhattacharjee, A. M. Gonzalez-Suarez, L. G. Rigat Brugarolas, U. Nallapati, J. Samitier, C. DeForest, F. Posas, J. L. Garcia-Cordero and A. Folch, *Lab Chip*, 2016, **16**, 2287–2294.

- 48 Y. Zheng, J. Chen and J. A. Lopez, *Thromb. Res.*, 2014, **133**, 525–531.
- 49 A. S. Popel and P. C. Johnson, *Annu. Rev. Fluid Mech.*, 2005, **37**, 43–69.
- 50 C. Michiels, *J. Cell. Physiol.*, 2003, **196**, 430–443.
- 51 J. W. Nichol, S. T. Koshy, H. Bae, C. M. Hwang, S. Yamanlar and A. Khademhosseini, *Biomaterials*, 2010, **31**, 5536–5544.
- 52 M. Djabourov, J. P. Lechaire and F. Gaill, *Biorheology*, 1993, **30**, 191–205.
- 53 H. Lee, W. Park, H. Ryu and N. L. Jeon, *Biomicrofluidics*, 2014, **8**, 54102.
- 54 V. Liu Tsang, A. A. Chen, L. M. Cho, K. D. Jadin, R. L. Sah, S. DeLong, J. L. West and S. N. Bhatia, *FASEB J.*, 2007, **21**, 790–801.
- 55 P. Thévenaz, U. E. Ruttimann and M. Unser, *IEEE Trans. Image Process.*, 1998, **7**, 27–41.
- 56 J. Schindelin, I. Arganda-Carreras, E. Frise, V. Kaynig, M. Longair, T. Pietzsch, S. Preibisch, C. Rueden, S. Saalfeld, B. Schmid, J.-Y. Tinevez, D. J. White, V. Hartenstein, K. Eliceiri, P. Tomancak and A. Cardona, *Nat. Methods*, 2012, **9**, 676–82.
- 57 E. K. U. Larsen, M. B. L. Mikkelsen and N. B. Larsen, *Biomicrofluidics*, 2014, **8**, 64127.
- 58 L. R. G. Treloar, *The physics of rubber elasticity*, Oxford University Press, 3rd edn., 1975.

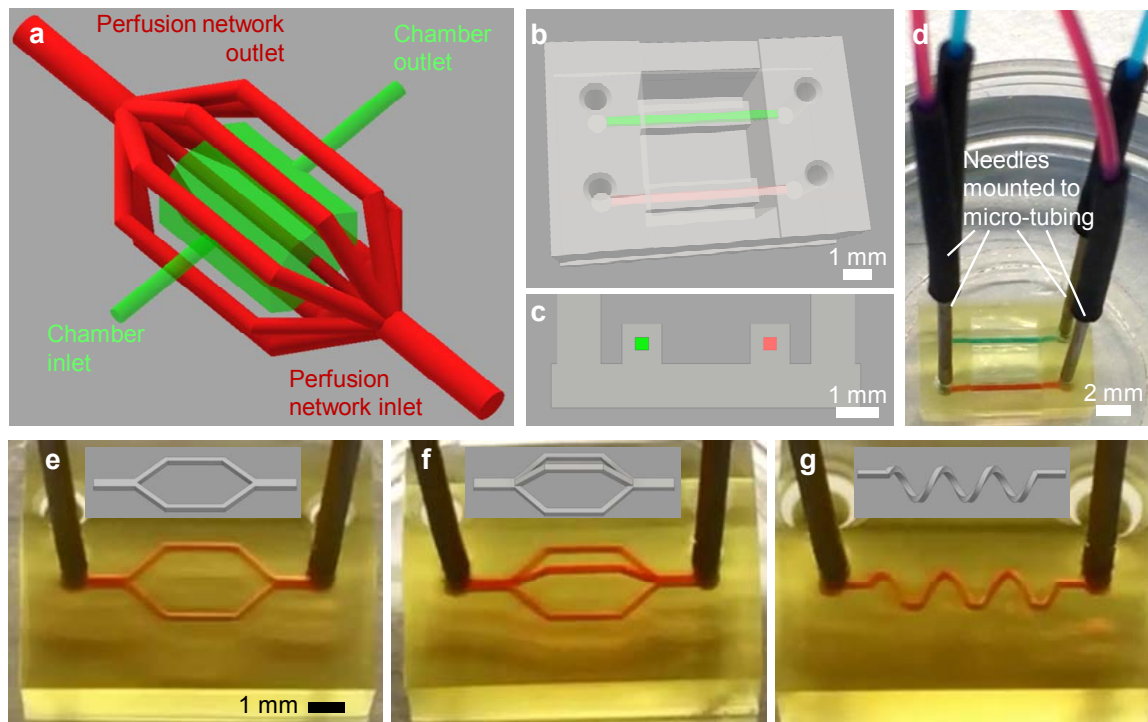


Fig. 1 (a) Schematic of a generic 3D cell culture chamber (green) surrounded and traversed by a medium perfusion network (red). (b,c) Design of a dual-channel model in perspective (b) and in cross-section (c) with square channels of side length $300\ \mu\text{m}$. (d) Printed PEGDA dual-channel construct perfused with separate dyed liquids simultaneously. (e-g) Optical micrographs of 3D printed and perfused PEGDA channel networks ($200\ \mu\text{m} \times 200\ \mu\text{m}$ square channel cross-section) of increasing 3D complexity from (e) dual planar configuration, (f) triple 3D geometry to (g) spiral geometry. The inserts show the respective CAD designs.

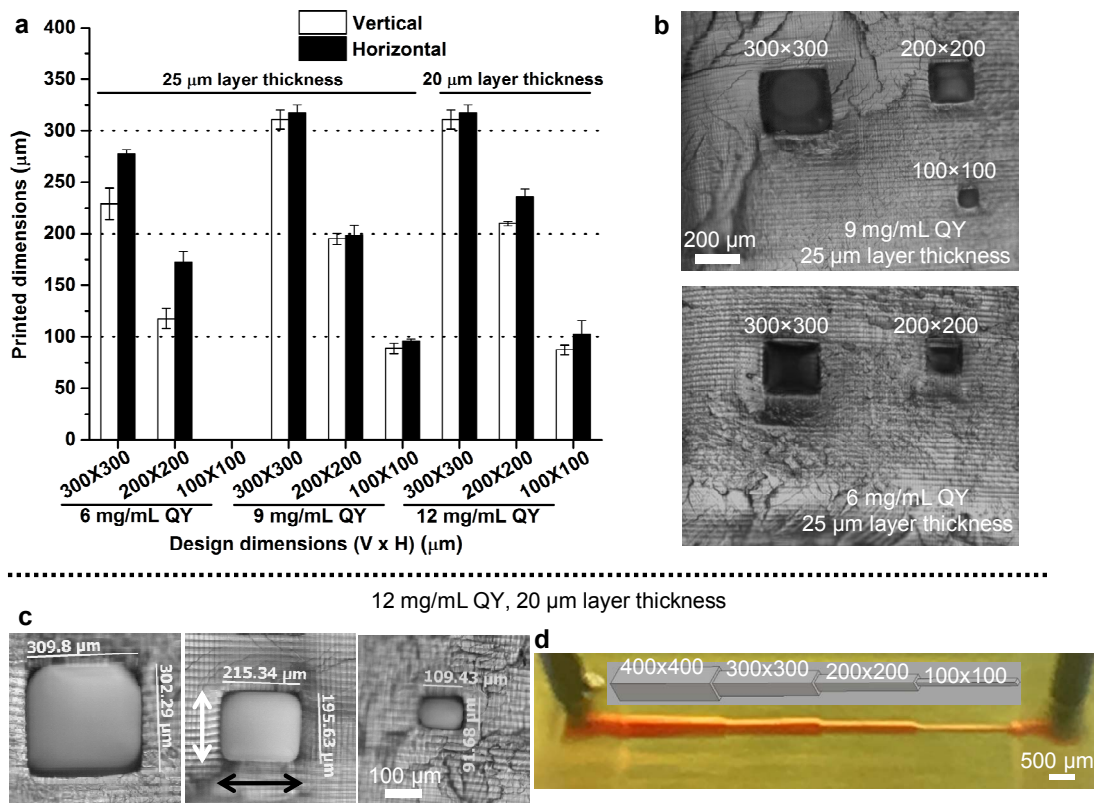


Fig. 2 (a-c) Measured printed channel dimensions versus design dimensions (error bars show the standard deviation, $n = 3$) from optical micrographs of sectioned horizontal channels with square cross-sections of decreasing dimensions using: different absorber concentrations yet the same layer thickness (b) and optimized resin formulation (c). (d) Stepwise narrowing channel with square cross-section from $400 \mu\text{m} \times 400 \mu\text{m}$ to $100 \mu\text{m} \times 100 \mu\text{m}$ printed in PEGDA using optimized resin formulation and perfused with dyed fluid. The insert shows the design of the narrowing channel.

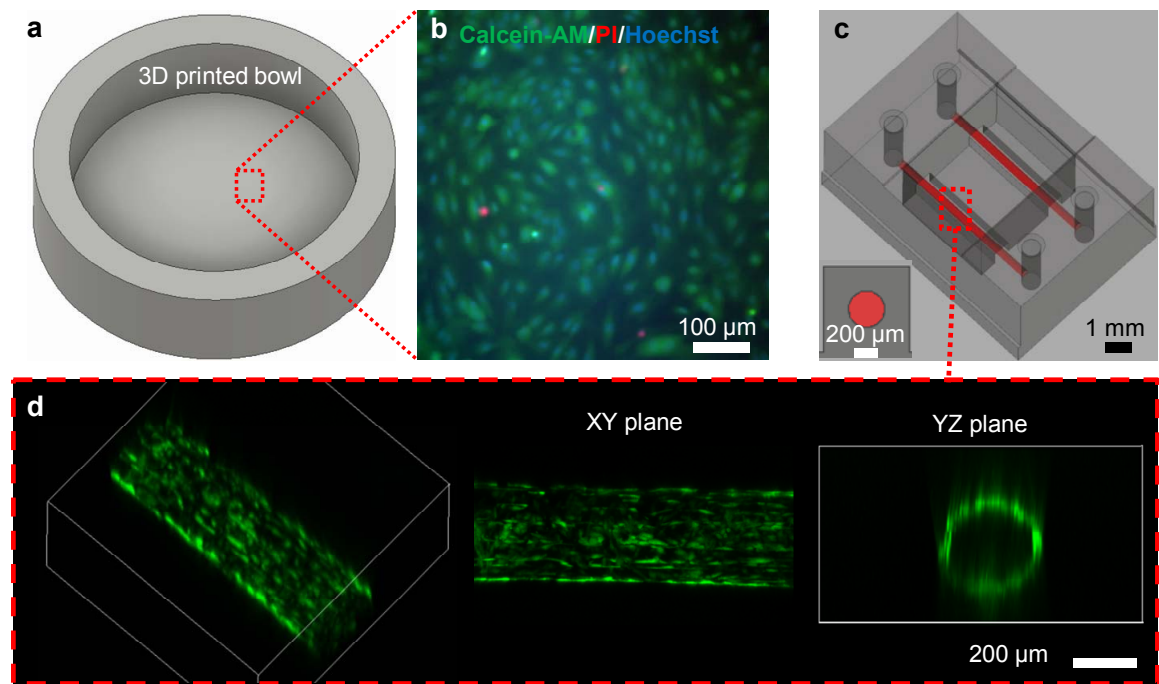


Fig. 3 (a) CAD design of bowl structure. (b) Composite fluorescence micrographs of HUVEC cells 24 h after being seeded in the printed PEGDA bowl structure surface functionalized with GelMA: live cells (calcein-AM, green), dead cells (propidium iodide, red) and nuclei (Hoechst 33342, blue). The seeding density was 7×10^4 cells cm^{-2} . (c) Design of a dual-channel model with cylindrical $\text{\O} 300 \mu\text{m}$ channels, with the insert showing the channel cross-section in red. (d) Confocal laser scanning micrographs of live HUVEC cells lining the printed and functionalized PEGDA micro-channel walls.

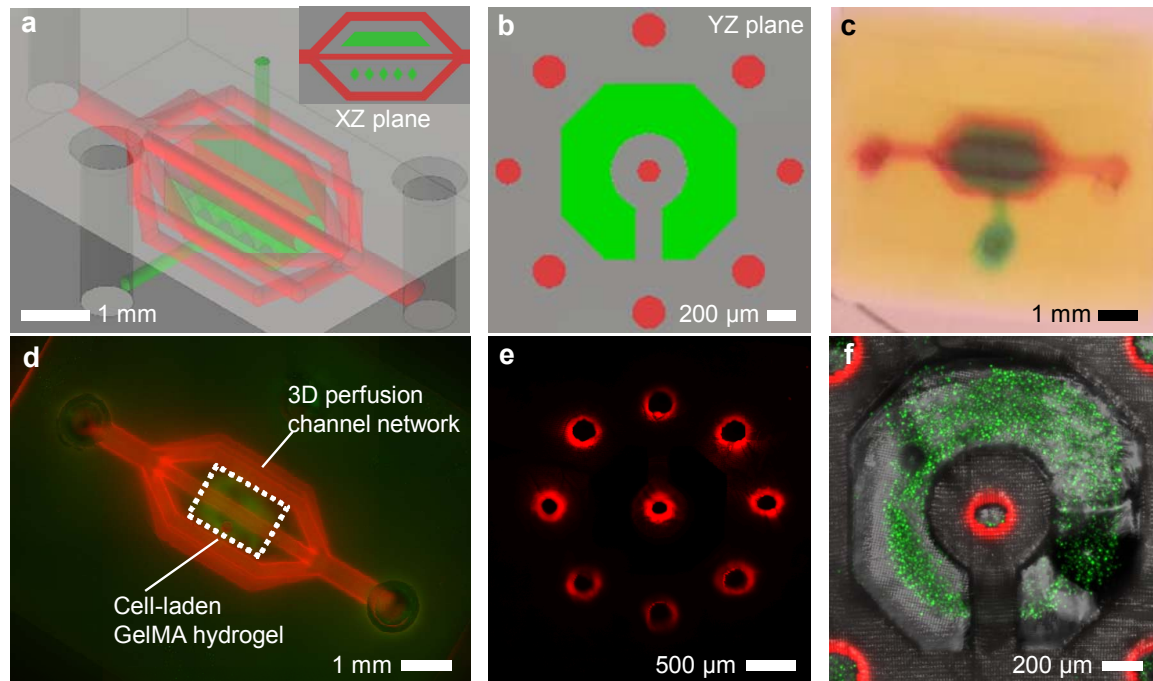


Fig. 4 (a,b) Design of a culture chamber with 8 surrounding and one central traversing vascular channels (a) and its corresponding cross-sectional view in the YZ plane (b). The insert in (a) shows the cross-sectional view in the XZ plane. (c) Photograph (top view) of the printed PEGDA construct with the vascular network perfused by red dyed liquid and the chamber perfused by blue dyed liquid. (d) Fluorescence micrograph (top view) of the construct with the vascular network walls coated by rhodamine (red) and the chamber filled with GelMA hydrogel laden with live fibroblasts (calcein AM, green). (e) Confocal fluorescence micrograph (rhodamine, red) of a cross-sectioned slice of the construct showing perfusing of all branched channels. (f) Confocal fluorescence micrograph of a cross-sectioned slice of the construct showing the perfused vascular network (rhodamine, red), live 3T3 fibroblasts (green) and the PEGDA construct outline (transmitted light, gray).